

Universal quantum melting of quasiperiodic attractors in driven-dissipative cavities

Caroline Nowoczyn,^{1,2} Ludwig Mathey,^{1,2} and Kilian Seibold³

¹*Center for Optical Quantum Technologies and Institute for Quantum Physics,
University of Hamburg, Hamburg 22761, Germany*

²*The Hamburg Center for Ultrafast Imaging, Hamburg 22761, Germany*

³*Department of Physics, University of Konstanz, 78464 Konstanz, Germany*

(Dated: July 8, 2025)

Nonlinear classical mechanics has established countless intriguing and profound phenomena. These include limit tori defined by toroidal attractors that support quasiperiodic motion of at least two incommensurate frequencies. Here we address the question, whether and how such phenomena persist in open quantum systems. We develop a quantum description of limit tori within the Lindblad master-equation formalism for a system of two coupled driven-dissipative Kerr cavities. Using the spectral theory of the Liouvillian and the truncated Wigner approximation, we analyze the system across the quantum-to-classical transition. In the classical limit, we identify two pairs of purely imaginary Liouvillian eigenvalues, corresponding to persistent quasiperiodic modes of the limit torus. Quantum fluctuations induce small negative real parts to these eigenvalues, giving rise to finite lifetimes of these modes. The corresponding Liouvillian gaps vanish algebraically in the classical limit. This behavior signals a genuine continuous dynamical phase transition, marked by the spontaneous breaking of time-translational symmetry. Analysis of individual quantum trajectories reveals quantum-fluctuation-induced dephasing as the primary mechanism behind this “quantum melting” of the torus. We quantify this dephasing using a circular-variance-based order parameter, revealing universal scaling with both system size and time. These scaling laws are robust and independent of microscopic parameters. Our results establish the quantum melting of limit tori as a distinct non-equilibrium critical phenomenon and provide concrete signatures for experimental observation in trapped ions and superconducting circuits.

I. INTRODUCTION

Nonlinear classical mechanics has provided a framework for understanding phenomena such as bistability, chaos, synchronization, and robust periodic motion [1–20]. Such dynamics are analyzed using tools like bifurcation theory [21, 22], Floquet analysis [23], and Lyapunov spectra [24], which reveal the stability and structure of underlying attractors. Among these attractors, limit tori—quasiperiodic motion characterized by trajectories that densely fill a toroidal manifold due to two or more incommensurate frequencies—emerge through Neimark-Sacker bifurcations [25–30]. These structures appear across disciplines, including fluid dynamics, nonlinear optics, chemistry, and biology [31–36]. Although limit tori are well-understood in classical systems, their quantum analogues have received little theoretical study, with only a few recent works [29].

Recent advances in driven-dissipative quantum platforms—such as superconducting circuits [37], ultracold atomic platforms [30, 38] and trapped-ion platforms—have opened new possibilities for investigating nonlinear dissipative quantum dynamics. Examples including quantum synchronization [10–12, 15, 16, 18–20] and time-crystalline behavior [39–43] show that many-body quantum systems can maintain long-lived coherence despite strong dissipation.

In this work, we address the question of how phenomena established in classical nonlinear mechanics translate into quantum dissipative dynamics. As an intriguing representative example we focus on limit tori.

We note that while other phenomena such as limit cycles [16, 17, 42, 44, 45] and emergent signatures of quantum chaos [46–50] have been explored in the quantum domain, the quantum description, and generally the fate of limit tori and complex attractors, are essentially unexplored. Quantum coherence, fluctuations, and dissipation can drastically reshape or destabilize such structures, raising fundamental questions about their persistence in open quantum systems. We consider the following questions:

- (a) Can quasiperiodic attractors survive quantum noise and dissipation?
- (b) What are the spectral signatures of quasiperiodic attractors in the Liouvillian?
- (c) Do universal laws govern the dephasing and disappearance of quasiperiodic attractors in the quantum regime?

Answering these questions is crucial for bridging classical nonlinear dynamics with the physics of open quantum systems. To address these questions on a concrete example, we develop a quantum description of limit tori and their associated Liouvillian spectrum in a minimal model of two coupled driven-dissipative Kerr cavities. By combining mean-field analysis, Liouvillian spectral theory [51–53], and quantum trajectory methods within the truncated Wigner approximation [54–58], we investigate the emergence, stability, and quantum melting—i.e., the quantum-fluctuation-induced degradation—of limit tori across the quantum-to-classical crossover. We identify

quasiperiodic motion via pairs of complex-conjugate Liouvillian eigenvalues whose real parts vanish in the classical limit, with Liouvillian gaps that close algebraically. This spectral signature reveals universal scaling laws governing the quantum melting, and supports its interpretation as a continuous dissipative phase transition [59].

The paper is organized as follows. In Sec. II, we introduce the model and theoretical framework. In Sec. III, we present our results on the emergence and melting of quantum limit tori and identify associated universal scaling laws. In Sec. IV, we discuss prospects for experimental realization, outlining a concrete implementation strategy in a trapped-ion platform. Finally, Sec. V summarizes our findings and discusses future directions.

II. THEORETICAL FRAMEWORK

Coupled Kerr cavities—We consider a minimal theoretical model of two coupled Kerr cavities, subject to incoherent driving and two-photon loss processes, as illustrated in Fig. 1(a). The Hamiltonian of the system reads

$$\frac{\hat{\mathcal{H}}}{\hbar} = \sum_{k=1,2} \omega_k \hat{a}_k^\dagger \hat{a}_k + \frac{U_k}{2} \hat{a}_k^{\dagger 2} \hat{a}_k^2 - J(\hat{a}_1^{\dagger 2} \hat{a}_2 + \hat{a}_2^{\dagger 2} \hat{a}_1), \quad (1)$$

where \hat{a}_k (\hat{a}_k^\dagger) are the bosonic annihilation (creation) operators for cavity k , satisfying the commutation relation $[\hat{a}_j, \hat{a}_k^\dagger] = \delta_{jk}$, ω_k denotes the bare cavity frequencies, U_k the strength of the on-site Kerr nonlinearities, and J the amplitude of the nonlinear tunneling term. Throughout this work, we refer to the excitations as “photons” for simplicity, though in specific implementations, such as the trapped-ion realization, discussed in Sec. IV, they may represent other bosonic modes, such as phonons.

The dissipative dynamics of the system is given by the Lindblad master equation for the density matrix $\hat{\rho}$ [60, 61]:

$$\frac{d\hat{\rho}}{dt} = \mathcal{L}\hat{\rho} = \frac{1}{i\hbar}[\hat{\mathcal{H}}, \hat{\rho}] + \sum_{k=1,2} \gamma_k \mathcal{D}[\hat{a}_k^\dagger]\hat{\rho} + \eta_k \mathcal{D}[\hat{a}_k^2]\hat{\rho}, \quad (2)$$

where $\mathcal{D}[\hat{L}]\hat{\rho} = \hat{L}\hat{\rho}\hat{L}^\dagger - \frac{1}{2}(\hat{L}^\dagger\hat{L}\hat{\rho} + \hat{\rho}\hat{L}^\dagger\hat{L})$ denotes the dissipator in Lindblad form associated with jump operator \hat{L} . Here, γ_k and η_k represent the incoherent pumping and two-photon loss rates, respectively. Unless otherwise specified, we consider the symmetric parameter choice $\omega_1 = \omega_2 = \omega = 1$, $U_1 = U_2 = 0.1$, $J = 0.4$, $\gamma_1 = \gamma_2 = \gamma = 1$, and $\eta_1 = \eta_2 = \eta = 1$. These values enable the emergence of complex dynamics, including limit cycles (LC) and limit tori (LT).

Spectral analysis of the Liouvillian—The dynamics of an open quantum system is governed by the Liouvillian superoperator \mathcal{L} , defined in Eq. (2), which acts on the system’s density matrix. Its spectrum is defined by the eigenvalue equation $\mathcal{L}\hat{\rho}_j = \lambda_j \hat{\rho}_j$, where λ_j are generally complex-valued. According to Spohn’s theorem [62–64],

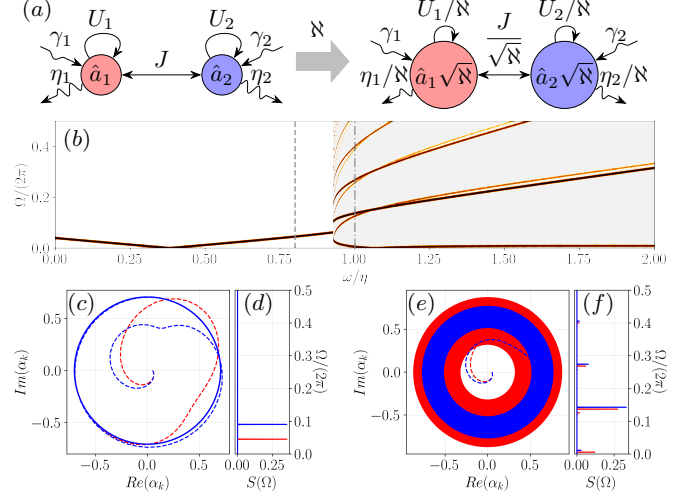


FIG. 1. Coupled, driven-dissipative Kerr cavities, described by Eqs. (1) and (2). (a) Schematic representation of the coupled Kerr cavities, and the quantum-to-classical rescaling of the system. The parameter \aleph is a dimensionless parameter, controlling the quantum-to-classical rescaling, see Eq. (4). (b) Heatmap of the power spectrum $S(\Omega)$ of mode 1, based on mean-field dynamics, as a function of ω , illustrating the number of frequencies contributing to the dynamics. The region with a white background corresponds to limit cycle dynamics, while the gray background indicates limit torus regime. The gray dashed line marks the frequency $\omega = 0.8$ for the limit cycle, shown in (c-d), and the dashed-dotted line marks the frequency $\omega = 1.0$ for the limit torus dynamics, shown in (e-f). (c) and (e) Phase-space trajectories of the mean fields α_1 (red) and α_2 (blue) obtained from the Gross-Pitaevskii (GP) equations as given in Eq. (3). (d) and (f) Spectra of modes 1 and 2, respectively. The depicted trajectories are obtained by numerically integrating the GP equations up to $\eta t = 10^4$. The other parameters are fixed at $U_1 = U_2 = 0.1$, $J = 0.4$, $\gamma_1 = \gamma_2 = \gamma = 1$, and $\eta_1 = \eta_2 = \eta = 1$.

any finite-dimensional open quantum system admits a unique nonequilibrium steady state (NESS) associated with the eigenvalue $\lambda_0 = 0$, while all other eigenvalues have strictly negative real parts. Consequently, any initial state asymptotically relaxes to the NESS. The timescale of this relaxation is set by the Liouvillian gap—the nonzero eigenvalue with the smallest magnitude of the real part [52]. The closing of the Liouvillian gap signals a qualitative change in the long-time dynamics, marking the onset of critical phenomena such as dissipative phase transitions or the emergence of persistent oscillations in the steady-state [42].

Quantum-to-classical rescaling—In the limit of large photon occupation, the dynamics of a driven-dissipative system can be described by the Gross-Pitaevskii equation (GPE), a mean-field approach that neglects quantum fluctuations. The GPE is obtained from the adjoint master equation of Eq. (2) by applying the mean-field approximation $\langle \hat{A}\hat{B} \rangle = \langle \hat{A} \rangle \langle \hat{B} \rangle$ and taking the classical

limit $\hbar \rightarrow 0$. It reads

$$\begin{aligned} i \frac{d\alpha_1}{dt} &= \left(\omega_1 + i \frac{\gamma_1}{2} + (U_1 - i\eta_1)|\alpha_1|^2 \right) \alpha_1 - 2J\alpha_1^* \alpha_2 \\ i \frac{d\alpha_2}{dt} &= \left(\omega_2 + i \frac{\gamma_2}{2} + (U_2 - i\eta_2)|\alpha_2|^2 \right) \alpha_2 - J\alpha_1^2 \end{aligned} \quad (3)$$

where $\alpha_k = \text{Tr}(\hat{a}_k \hat{\rho})$ denotes the expectation value of the annihilation operator. To systematically control the crossover between quantum and classical behavior, we introduce a scaling parameter \aleph , which rescales the system parameters and operators according to

$$U_k = \frac{\tilde{U}_k}{\aleph}, \quad J = \frac{\tilde{J}}{\sqrt{\aleph}}, \quad \eta_k = \frac{\tilde{\eta}_k}{\aleph} \quad \text{and} \quad \hat{a}_k \rightarrow \hat{a}_k \sqrt{\aleph} \quad (4)$$

as illustrated in Fig. 1(a). Under this transformation, the complex fields scale as $\alpha_k = \tilde{\alpha}_k \sqrt{\aleph}$, leading to mean-field populations $n_k = |\alpha_k|^2 \propto \aleph$. Notably, Eq. (3) remains invariant under these scaling relations, demonstrating that the limit $\aleph \rightarrow \infty$ defines a well-controlled classical limit characterized by an infinite number of photons. This scaling method is commonly used in the study of driven-dissipative quantum systems to systematically explore quantum-to-classical transitions [65–70].

Truncated Wigner approximation—To capture quantum fluctuations and the mixed character of the density matrix beyond mean-field theory, we employ the truncated Wigner approximation (TWA) [55, 56]. In the TWA, the density operator $\hat{\rho}$ is mapped onto the Wigner quasiprobability distribution $W(\{\alpha_k, \alpha_k^*\})$ over the real and imaginary parts of the complex mode amplitudes α_k . Truncating the dynamical equations for the Wigner distribution at order $\mathcal{O}(\hbar^2)$ yields a Fokker-Planck equation, see Supplemental Material [71], which is equivalent to the ensemble dynamics of stochastic Langevin trajectories.

For the two-cavity model, we initialize the Wigner function with the distribution corresponding to a two-mode coherent state $|\alpha_1(0), \alpha_2(0)\rangle$. The Langevin equations for the rescaled fields $\tilde{\alpha}_k$ take the form:

$$\begin{aligned} i \frac{d\tilde{\alpha}_1}{dt} &= \left[\omega_1 + i \frac{\gamma_1}{2} + (\tilde{U}_1 - i\tilde{\eta}_1) \left(|\tilde{\alpha}_1|^2 - \frac{1}{\aleph} \right) \right] \tilde{\alpha}_1 \\ &\quad - 2\tilde{J}\tilde{\alpha}_1^* \tilde{\alpha}_2 + \sqrt{\frac{\gamma_1}{2\aleph}} \chi_1(t) + \sqrt{\frac{2\tilde{\eta}_1 |\tilde{\alpha}_1|^2}{\aleph}} \xi_1(t) \\ i \frac{d\tilde{\alpha}_2}{dt} &= \left[\omega_2 + i \frac{\gamma_2}{2} + (\tilde{U}_2 - i\tilde{\eta}_2) \left(|\tilde{\alpha}_2|^2 - \frac{1}{\aleph} \right) \right] \tilde{\alpha}_2 \\ &\quad - \tilde{J}\tilde{\alpha}_1^2 + \sqrt{\frac{\gamma_2}{2\aleph}} \chi_2(t) + \sqrt{\frac{2\tilde{\eta}_2 |\tilde{\alpha}_2|^2}{\aleph}} \xi_2(t), \end{aligned} \quad (5)$$

where χ_k and ξ_k are independent, zero-mean and unit-variance complex Gaussian stochastic variables, characterized by correlation functions $\langle \chi_k(t) \chi_{k'}(t') \rangle = \langle \xi_k(t) \xi_{k'}(t') \rangle = 0$, $\langle \chi_k^*(t) \chi_{k'}(t') \rangle = \delta_{k,k'} \delta(t-t')$, and $\langle \xi_k^*(t) \xi_{k'}(t') \rangle = \delta_{k,k'} \delta(t-t')$. The noise terms $\chi_k(t)$ and $\xi_k(t)$ account for quantum fluctuations. The expectation value of an observable \hat{O} is approximated by averaging

its Weyl symbols $O_W(\{\alpha_k, \alpha_k^*\})$ over N_{traj} stochastic trajectories:

$$\langle \hat{O} \rangle(t) \approx \frac{1}{N_{\text{traj}}} \sum_{\mu=1}^{N_{\text{traj}}} O_W(\{\alpha_{k,\mu}(t), \alpha_{k,\mu}^*(t)\}) \quad (6)$$

where the individual stochastic realizations are labeled by μ . In particular, for symmetrically, i.e., Weyl-ordered products of operators, such as $\mathcal{S}[(\hat{a}_i^\dagger)^n \hat{a}_j^m]$, the expectation value reads:

$$\langle \mathcal{S}[(\hat{a}_i^\dagger)^n \hat{a}_j^m] \rangle(t) \approx \frac{1}{N_{\text{traj}}} \sum_{\mu=1}^{N_{\text{traj}}} (\alpha_{i,\mu}^*(t))^n (\alpha_{j,\mu}(t))^m \quad (7)$$

The system is initialized with each mode prepared in a coherent state of amplitude $\tilde{\alpha}_0 = 0.05$. The initial conditions for the stochastic trajectories are sampled from the corresponding Gaussian Wigner distribution,

$$\tilde{\alpha}_k(t=0) = \tilde{\alpha}_0 + \frac{1}{\sqrt{2\aleph}} \zeta_k, \quad (8)$$

where ζ_k is a unit-variance complex random variable with zero mean, satisfying $\langle \zeta_k \zeta_{k'} \rangle = 0$ and $\langle \zeta_k^* \zeta_{k'} \rangle = \delta_{k,k'}$. Each realization corresponds to a possible measurement outcome, providing a semi-classical picture of the system's quantum dynamics.

III. QUANTUM MELTING OF LIMIT TORI AND ITS UNIVERSALITY

A. Quantum melting of LT dynamics

Mean-field analysis—We begin by analyzing the mean-field dynamics to identify parameter regimes where LC and LT attractors emerge. Figure 1(b) shows the power spectrum $S(\Omega)$ of mode 1, computed from the GPE, as a function of ω . On the left side of the plot, with white background, a single dominant frequency is visible, signaling LC behavior, while on the right, with gray background, the presence of two fundamental incommensurate frequencies signals the LT phase, characterized by quasiperiodic dynamics. A Lyapunov exponent analysis confirms this distinction. The LC phase shows a single zero Lyapunov exponent, while the LT phase is marked by two zero exponents, see Supplemental Material [71]. The phase-space trajectories further illustrate the nature of the attractors. For $\omega = 0.8$, the system exhibits periodic oscillations with well-defined amplitude and frequency, see Fig. 1(c). For $\omega = 1$, the amplitude modulation over multiple periods reveals a toroidal structure, see Fig. 1(e). The ratio of the dominant frequencies is analyzed in the Supplemental Material [71].

Quantum transient—Individual stochastic TWA trajectories show that the LT dynamics observed in the

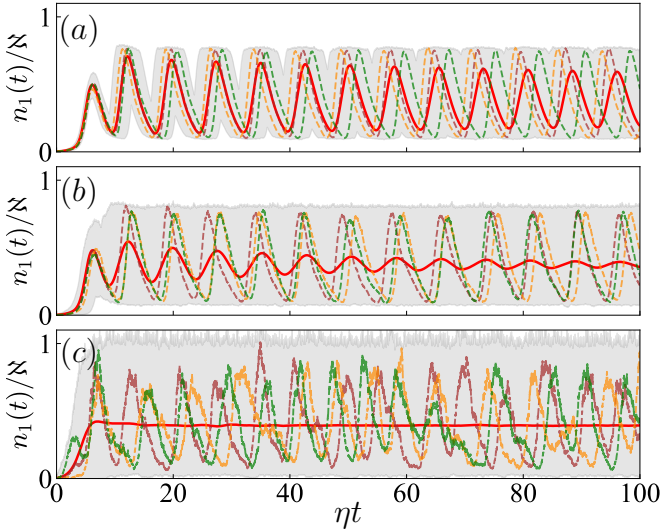


FIG. 2. Dynamics of the rescaled occupation $n_1(t)/N$ of mode 1, in the TWA. Panels (a)—(c) correspond to decreasing values of the scaling parameter: (a) $N = 30000$, (b) $N = 4000$, (c) $N = 200$. Dashed lines show the evolution of individual TWA trajectories, while the solid red lines indicate the expectation value of $n_1(t)/N$. The gray area represents the range between the minimal and maximal occupation values across all trajectories. Both modes are initialized in a coherent state centered at $\tilde{\alpha}_0 = 0.05$. The expectation values are averaged over 3×10^4 TWA trajectories. Mode 2 shows qualitatively similar behavior.

mean-field regime persist in the quantum regime. Figure 2 shows the time evolution of single-trajectory dynamics, represented by dashed lines. After a rapid transient regime ($\eta t \lesssim 10$), each trajectory settles into the LT attractor and explores its full amplitude range without damping.

The gray-shaded area in Fig. 2 delineates the envelope of minimal and maximal occupations across all trajectories. Although quantum fluctuations are present, each individual trajectory stays within the envelope, maintaining dynamics that is confined to the LT attractor. They remain quasiperiodic, with persistent undamped oscillations. Over time, stochastic noise induces gradual dephasing between trajectories, leading to a decay of phase coherence across the ensemble of single trajectories. This results in an effective damping of ensemble-averaged TWA expectation values, as shown in Fig. 2, where the solid red lines depict the rescaled occupation $n_1(t)/N$ approaching a non-oscillatory steady state. The progressive temporal broadening of the envelope (gray-shaded area) in Fig. 2(a) further reflects the dephasing dynamics. This process constitutes the dominant relaxation mechanism and is governed by the Liouvillian gap: quantum noise induces random phase drift, effectively melting the LT.

Liouvillian spectral signature of LT—As discussed above, at the mean-field level, the two coupled driven-dissipative Kerr cavities in our model undergo a Neimark-

Sacker bifurcation, giving rise to a two-dimensional LT attractor embedded in four-dimensional phase space. This attractor is characterized by exactly two vanishing Lyapunov exponents—one for each angular degree of freedom—while all other exponents are strictly negative. The resulting quasiperiodic dynamics are governed by two incommensurate frequencies, a hallmark of toroidal motion. These classical features leave a clear imprint on the quantum dynamics. Specifically, the emergence of LTs is encoded in the spectral structure of the Liouvillian superoperator \mathcal{L} . The low-lying spectrum encodes two key ingredients: the quasiperiodic motion inherited from mean-field dynamics, and the slow dephasing induced by quantum fluctuations.

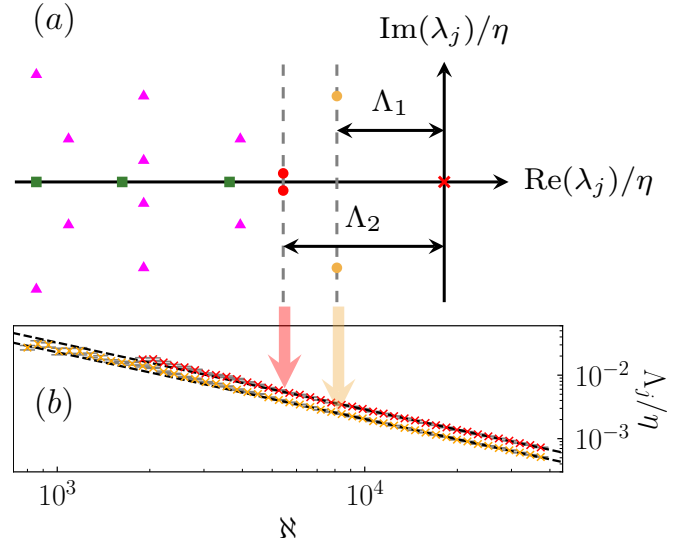


FIG. 3. Liouvillian spectrum analysis. (a) Schematic representation of the spectrum of the Liouvillian. A zero eigenvalue, indicated with a red cross, corresponds to the unique steady state. In the LT regime, two pairs of complex conjugate eigenvalues (red and gold) emerge, each with small real parts that vanish in the classical limit and incommensurate imaginary parts. (b) Scaling of the Liouvillian gaps with N . The power-law fits of the two Liouvillian gaps for $5 \times 10^3 \leq N \leq 4 \times 10^4$ is shown by the dashed and dash-dotted lines. The coefficients of the fit are $\Lambda_j/\eta = N^{-a_j} \times b_j$, with $a_1 = 1.054 \pm 0.01$ and $b_1 = 47.144 \pm 5.724$ and $a_2 = 1.052 \pm 0.01$ and $b_2 = 32.922 \pm 3.452$.

Figure 3(a) schematically illustrates this structure of the low-lying Liouvillian spectrum. The steady state corresponds to a unique zero eigenvalue $\lambda_0 = 0$, denoted as a red cross, as required by Lindblad formalism. In a LC regime, the Liouvillian spectrum is dominated by a single pair of complex conjugate eigenvalues. The imaginary parts of these eigenvalues determine the oscillation frequency. The small negative real parts set the decay rate, which vanishes in the classical limit where quantum fluctuations are negligible [42, 45]. By contrast, the low-lying Liouvillian spectrum of a LT comprises two sets of

complex conjugate eigenvalues

$$\lambda_j^\pm = -\Lambda_j \pm i\nu_j \quad \text{for } j = 1, 2, \quad (9)$$

with incommensurate frequencies $\nu_{1,2}$ associated with motion along the two angular directions of the torus. Each direction is subject to quantum-fluctuation-induced dephasing, quantified by a distinct Liouvillian gap Λ_j . In the classical limit, where $\Lambda_j \rightarrow 0$, this leads to two sets of purely imaginary eigenvalues, recovering the undamped quasiperiodic motion.

To probe the resulting quasiperiodicity in cavity 1, we compute its time-resolved emission spectrum via a windowed Fourier transform of the first-order correlation function:

$$S_1(t, \Omega) = 2\text{Re} \int_0^\infty d\tau w(t-\tau) \langle \hat{a}_1^\dagger(t_0+\tau) \hat{a}_1(t_0) \rangle e^{i\Omega\tau}, \quad (10)$$

with window function $w(s)$. This quantity is numerically evaluated using a discrete short-time Fourier transform of the correlation function sampled from $N_{\text{traj}} = 10^5$ TWA trajectories, see Supplemental Material [71].

The resulting spectrogram displays two dominant peaks at constant incommensurate frequencies $\nu_{1,2}$, with magnitudes decaying over time. The decay rates are determined by the respective Liouvillian gaps $\Lambda_{1,2}$, thus

providing a direct probe of the Liouvillian spectrum. Since the observable we analyze is only sensitive to the dynamics of cavity 1, spectral features associated with cavity 2 are not resolved. Nevertheless, cavity 2 contributes a secondary structure in the Liouvillian spectrum, comprising an additional pair of complex conjugate eigenvalues linked to its own quasiperiodic motion. Figure 3(b) shows the scaling of Λ_j with scaling parameter \aleph . We find *power-law* behavior,

$$\Lambda_j \propto \aleph^{-a_j}, \quad a_j \approx 1. \quad (11)$$

This scaling establishes a direct connection between phase diffusion—arising from the fine-grained dynamics of individual trajectories—and the relaxation rates of ensemble-averaged observables. In particular, the inverse gaps $1/\Lambda_j$ set the slowest timescales over which quasiperiodic oscillations in single-trajectory observables lose phase coherence, and is directly linked to the relaxation of population oscillations in Fig. 2. The algebraic gap closing reflects diffusive phase decoherence along each angular coordinate, with a diffusion constant scaling as $D \propto \aleph^{-1}$. Accordingly, each Liouvillian gap behaves as $\Lambda_j \approx D \propto \aleph^{-1}$. When probing an observable sensitive to *both* angular directions (e.g. $S_1(\omega)$), the total dephasing rate becomes $\Lambda_1 + \Lambda_2 \approx 2D$, preserving the \aleph^{-1} scaling.

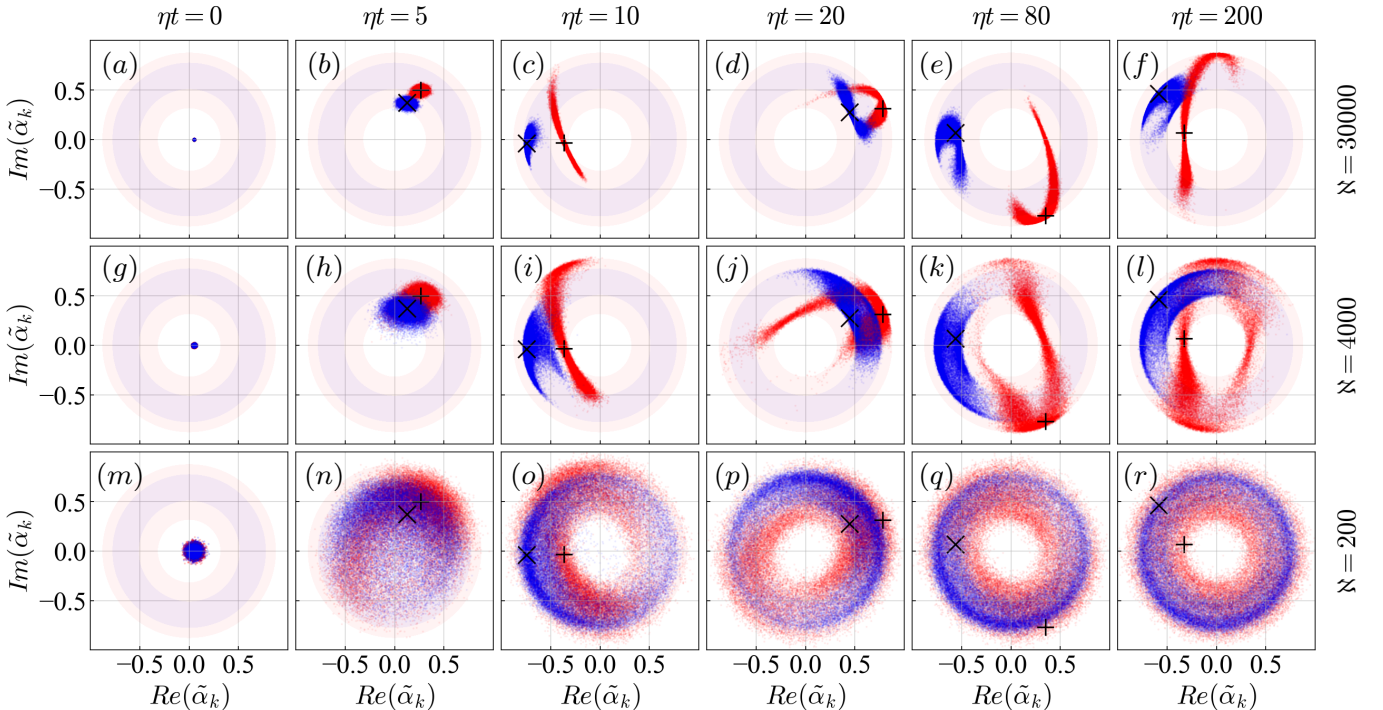


FIG. 4. Wigner function reconstructions based on the TWA fields α_1 (red) and α_2 (blue), shown for different times t (columns) and scaling parameter \aleph (rows). Classical GPE solutions for mode 1 marked with +, and mode 2 marked with \times are shown at corresponding times. The background light red and light blue regions indicate the phase-space area traced by the classical LT attractor, as obtained from GPE simulations. The three values of \aleph match those in Fig. 2, decreasing from the top to the bottom row. Each distribution is obtained from 3×10^4 TWA trajectory realizations.

This power-law scaling can also be understood from signal-to-noise ratio (SNR) considerations: the coherent amplitude scales as $|\alpha| \propto \sqrt{\aleph}$, while quantum fluctuations remain \aleph -independent, leading to $\text{SNR} \sim \aleph$. Since phase diffusion is driven by quantum noise, dephasing rates scale inversely with SNR [72, 73], yielding $\Lambda_j \propto \aleph^{-1}$.

Crucially, the frequencies ν_j remain invariant with increasing \aleph , reflecting their mean-field origin. Indeed, they match the frequencies obtained from the spectrum of the GPE, confirming that the Liouvillian spectrum inherits the angular frequencies of the underlying quasiperiodic mean-field dynamics.

Importantly, the extracted scaling exponents $a_j \approx 1$ for the Liouvillian gaps Λ_j are found to be robust across different parameter regimes that support limit tori. This indicates that this scaling is a universal feature of the quantum-to-classical crossover in quasiperiodic open systems.

Quantum melting—The quantum melting of the LT structure is further illustrated through Wigner function reconstructions presented in Fig. 4. The reconstructions are obtained from TWA fields α_1 (red) and α_2 (blue) for different times (columns) and scaling parameters \aleph (rows). For reference, the phase-space area of the classical LT obtained from the GPE, and also shown in Fig. 1(e), is overlaid as light red and light blue regions. Initially, the system is prepared according to Eq. (8) for both modes shown in the first column of Fig. 4. During time evolution, the Wigner distribution migrates towards the phase-space region of the LT, see second and further columns, circulating while remaining confined within the toroidal attractor. Remarkably, the distribution is well-confined to the phase-space region of the classical LT. Single trajectories remain confined in this structure, consistent with Fig. 2. The noise manifests itself along both temporal and scaling dimensions, depicted horizontally and vertically, respectively. At later times, dephasing at the level of single trajectories induces broadening of the Wigner function over the entire toroidal structure in both modes. Similarly, decreasing \aleph results in a broader distribution, indicating that quantum fluctuations speed up the diffusion process.

Robustness against single-photon loss and thermal noise—To ensure experimental relevance, we evaluated the robustness of our results against unavoidable single-photon loss and thermal fluctuations. These effects are incorporated into the master equation and TWA formalism, as detailed in the Supplemental Material [71]. We systematically analyzed how key quantities—such as Liouvillian gap and circular variance—are affected by these perturbations. These findings demonstrate that our conclusions remain valid under experimentally realistic levels of dissipation and thermal noise.

B. Universal scaling

Having established the emergence of LT and their melting via both trajectory dynamics and spectral signatures, we now investigate how coherence degrades as a function of time t and scaling parameter \aleph . In the following, we demonstrate that this melting follows universal scaling laws. To this end, we quantify phase diffusion in phase space via the circular variance,

$$R(t) = 1 - \left| \frac{1}{N_{\text{traj}}} \sum_{n=1}^{N_{\text{traj}}} e^{i\theta_n(t)} \right|, \quad (12)$$

where θ_n denotes the phase-space angle of the n th trajectory, and N_{traj} is the total number of trajectories. We note that the scaling parameter \aleph is closely related to the number of photons in the cavities. The metric in Eq. (12) exploits the intrinsic circular symmetry of the system dynamics in phase space, and serves as a sensitive measure of phase diffusion. For an ideally circular-invariant state, R solely and faithfully captures the dephasing dynamics. However, when the Wigner distribution deviates from perfect circular symmetry, see Fig. 4, oscillations in the mean phase-space angle emerge, thereby introducing an additional time-dependent modulation in R . As the deviation from perfect circular symmetry, and thus the oscillation in R , stem solely from the initialization—and are not associated with the melting of the LT structure—we mitigate their influence by introducing the period-averaged circular variance

$$\bar{R}(t) = \int_{t-T/2}^{t+T/2} d\tau R(\tau), \quad (13)$$

where T is the oscillation period of the mean phase-space angle. We compute $\bar{R}(\aleph, t)$ in cavity 1 over increasing values of the scaling parameter \aleph and time t , fitting the resulting curves to an exponential relaxation form, $\bar{R}(x) = 1 - \exp(-\delta_{\bar{R}}x)$, with x representing either time or the inverse scaling parameter $1/\aleph$. The relaxation rate $\delta_{\bar{R}}(x)$ thus plays an analogous role to the Liouvillian gap extracted earlier from the emission spectrum: both quantify the characteristic decay rate associated with the dephasing of coherent dynamics due to quantum noise. The relaxation rate $\delta_{\bar{R}}(x)$ is found to exhibit a power-law dependence, $\delta_{\bar{R}}(x) = cx^d$, with c and d positive constants. Figure 5 illustrates the scaling property of $\delta_{\bar{R}}(x)$. The time-dependence of $\bar{R}(\aleph, t)$ is displayed for five fixed values \aleph_j , while the dependence on the inverse scaling parameter $1/\aleph$ is shown for five fixed time points t_j . Rescaling the time and the $1/\aleph$ axis using the coefficients that characterize the power-law dependencies of $\delta_{\bar{R}}(t)$ and $\delta_{\bar{R}}(1/\aleph)$,

$$\begin{aligned} t &\rightarrow t' = (\aleph_j/\aleph_0)^{d_1} t \\ 1/\aleph &\rightarrow 1/\aleph' = (t_j/t_0)^{d_2} 1/\aleph \end{aligned} \quad (14)$$

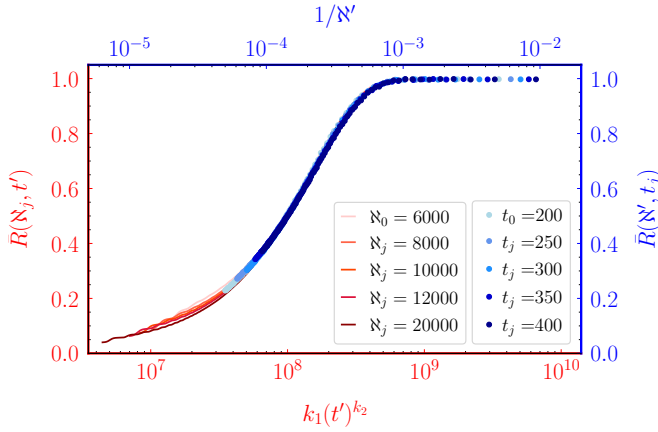


FIG. 5. Universal scaling behavior of the quantum-to-classical crossover. Data collapse of the period-averaged circular variance is achieved by plotting \bar{R} against (i) the rescaled time t' (red curves and axes), $\bar{R}(N_j, t')$, and (ii) the rescaled scaling parameter N' (blue curves and axes), $\bar{R}(N', t_j)$. The time (red) and inverse scaling parameter (blue) axes are rescaled according to Eq. (14), revealing a power-law dependence of the relaxation dynamic along both dimensions. Further rescaling the time axis according to Eq. (16), achieves an overall data collapse, highlighting the universality of the scaling behavior.

leads to a scaling collapse of the curves, with $d_1 \approx 1.08$ and $d_2 \approx 0.90$. We find that the two scaling dimensions—time and N —are intrinsically linked by the relation

$$t = \alpha N^\beta, \quad (15)$$

with $\alpha = (c_1/c_2)^{1/d_2} = 1.04 \pm 0.01$ and $\beta = d_1/d_2 = -1.196 \pm 0.001$. In Fig. 5, this universality is further demonstrated by a collapse of the data when Eq. (15) is used to rescale the time axis as

$$t' \rightarrow k_1(t')^{k_2}, \quad (16)$$

with $k_1 = (c_1/c_2)^{d_2/d_1-1} t_0^{d_2}/N_0^{d_1}$, $k_2 = -d_2/d_1$. This clearly shows that the rate of phase diffusion is inherently tied to the scaling parameter and quantum fluctuations. The scaling relation demonstrates a universal mechanism for the emergence of classical behavior from quantum dynamics, highlighting the universal nature of dephasing in quantum systems exhibiting LT dynamics.

C. Consistent indicators of quantum melting

We now demonstrate that the observables analyzed in Secs. III A and III B reflect the same underlying mechanism: quantum-fluctuation-induced dephasing of coherent torus dynamics. While conceptually distinct, the Liouvillian spectral gap and the phase diffusion measured by circular variance yield consistent scaling behavior. Specifically, the Liouvillian gap Λ_j extracted from the emission spectrum defined in Eq. (10) scales as N^{-a_j} ,

while the relaxation rate $\delta_{\bar{R}}$ of the period-averaged circular variance scales as N^{-d_1} . Both exponents are approximately unity, with $a_j \approx 1.05$ and $d_1 \approx 1.08$, as seen in Eq. (11). This agreement confirms that both observables capture the same fluctuation-driven relaxation process. Importantly, the spectral approach probes dissipation along each angular direction of the torus individually, while the circular variance captures global phase decoherence. The agreement between their scaling exponents therefore implies that quantum dephasing is isotropic across the torus manifold and that the underlying mechanism is universal.

This dual characterization not only strengthens the interpretation of LT melting as a universal, fluctuation-induced crossover, but also provides two experimentally accessible probes for identifying this regime. Furthermore, it demonstrates that the universal scaling law—revealed along one angular dimension of the LT via circular variance—applies uniformly across all toroidal directions. This reveals a deep structural invariance of the scaling, highlighting a new universality class for topologically nontrivial attractors in open quantum systems.

D. Quantum melting of LT as a dissipative phase transition

Based on the analysis of the Liouvillian spectrum, we describe how the gradual melting of LTs induced by increasing quantum fluctuations can be interpreted as a continuous dissipative phase transition.

Symmetry structure—The Hamiltonian Eq. (1) and the Liouvillian Eq. (2) are both invariant under a global continuous $U(1)$ symmetry

$$\hat{a}_1 \rightarrow e^{i\phi} \hat{a}_1, \quad \hat{a}_2 \rightarrow e^{2i\phi} \hat{a}_2. \quad (17)$$

Additionally, \mathcal{L} is invariant under continuous time translations, as it is explicitly time-independent. In the LT phase, three continuous generators are spontaneously broken: one $U(1)$ phase symmetry and two independent continuous time-translation symmetries to quasiperiodic oscillations at the incommensurate frequencies $\nu_{1,2}$. Applying the open-system Nambu-Goldstone theorem [74] to our model yields two diffusive modes associated with the spontaneous breaking of these three continuous symmetries. One of these modes is a “mixed” mode, resulting from a nonzero commutator between the $U(1)$ generator and one of the time-translation generators. The second mode corresponds to phase diffusion along the remaining torus angle. Moreover, for any finite system parameters, the Liouvillian generically possesses a unique, time-translationally invariant stationary state [51, 52, 64], indicating that all spontaneously broken symmetries are eventually restored at long times.

Goldstone-modes softening—In the classical limit $N \rightarrow \infty$, each incommensurate frequency of the LT corresponds to a spontaneously broken continuous time-translation symmetry [75, 76]. Accordingly, a two-

frequency torus supports two independent Goldstone modes, each associated with a distinct angular coordinate. Quantum fluctuations restore these symmetries, softening the Goldstone modes into damped modes with finite coherence times. This softening manifests in the Liouvillian spectrum: in the classical limit, each gapless Goldstone mode appears as a purely imaginary eigenvalue pair $\lambda_j^\pm = \pm i\nu_j$. Quantum corrections introduce small negative real parts, resulting in Liouvillian gaps Λ_j . These gaps quantify phase diffusion along the corresponding angular directions and define the finite lifetimes of the soft modes. This generalizes previous results for limit cycles [45, 77], where a single broken continuous time-translational symmetry gives rise to one soft mode. For LTs, the existence of two soft modes reflects the richer quasiperiodic symmetry-breaking structure.

Critical behavior—Dissipative critical phenomena are commonly classified into two classes based on Liouvillian gap closure: (i) exponential closing, associated with bistability and metastable switching, and (ii) algebraic closing, linked to critical diffusive modes and continuous (second-order) transitions [52, 67, 78]. Our results indicate that LT melting falls into the second class: the Liouvillian gaps Λ_j close algebraically as $\Lambda_j \propto \aleph^{-1}$, signaling diverging coherence times and critical slowing down of toroidal dynamics [79]. In contrast to first-order transitions, this crossover shows no bistability, hysteresis, or metastable coexistence. Instead, the system continuously deforms from a topological phase-space attractor into an incoherent, quantum-noise-dominated state. This behavior contrasts with the exponential gap scaling $\sim \exp(-c\aleph)$, and phase coexistence typical of first-order transitions [52, 67].

Two-dimensional scaling structure—Despite the system being $0 + 1$ -dimensional—zero spatial dimensions, plus time, we uncover a two-dimensional scaling structure in (\aleph, t) . A genuine dynamical critical point emerges in the limit $\aleph \rightarrow \infty$, even in the absence of spatial structure [79]. Simultaneously, the nontrivial scaling relation $t \sim \aleph^\beta$ show that time itself becomes a critical scaling dimension. The resulting dynamical scaling collapse signals the emergence of a universal behavior, echoing space-time scaling phenomena seen in Kosterlitz-Thouless transitions and quasi-long-range order in 2D condensates such as superfluids, where a genuine order arises only asymptotically in a singular limit (here, $\aleph \rightarrow \infty$).

Together, these findings establish LT melting as a universal dynamical crossover, governed by the softening of toroidal phase dynamics. This identifies a novel class of dynamical universality in open quantum systems, combining dissipative criticality, topological attractors, and fluctuation-driven decoherence in low-dimensional systems.

IV. EXPERIMENTAL REALIZATION

The driven-dissipative coupled Kerr oscillator system described by Eqs. (1) and (2) can be experimentally realized with trapped ions [10, 17]. In this realization, two motional modes of a single ion serve as the bosonic modes [80], offering precise control over system parameters and facilitating the study of quantum-to-classical transitions.

Motional modes and trapping potential—In a linear Paul trap, an ion experiences harmonic confinement along the orthogonal directions. By adjusting the trap potentials, one can achieve nearly degenerate motional frequencies, $\omega_1 \approx \omega_2$, as required for the model. The non-interacting Hamiltonian, including internal electronic states, is given by:

$$\frac{\hat{H}_0}{\hbar} = \omega_1 \hat{a}_1^\dagger \hat{a}_1 + \omega_2 \hat{a}_2^\dagger \hat{a}_2 + \sum_j \omega_{eg}^{(j)} |e_j\rangle \langle e_j|, \quad (18)$$

where $\omega_{eg}^{(j)}$ denotes the energy difference between the j th electronic excited state $|e_j\rangle$ and the electronic ground state $|g\rangle$.

Engineering Kerr nonlinearity—Anharmonicities in the trapping potential can be introduced with multipole trap designs or by applying tailored static electric fields [81–83], leading to a Kerr-type nonlinearity in the motional modes. In the interaction picture and under the rotating wave approximation (RWA), the quartic potential terms $\propto (\hat{a}_k + \hat{a}_k^\dagger)^4$ yield an effective Kerr interaction:

$$\frac{\hat{V}_I^{\text{RWA}}}{\hbar} \approx \frac{U_k}{2} \hat{a}_k^\dagger \hat{a}_k^\dagger \hat{a}_k \hat{a}_k, \quad (19)$$

where U_k is the Kerr coefficient, tunable via the trap's electric field configuration.

Nonlinear mode coupling—Nonlinear coupling between the two motional modes can be achieved through laser driving that induces two-phonon and single-phonon transitions via an intermediate electronic state $|e_j\rangle$ [17]. This is achieved by applying two laser fields that off-resonantly drive the second red sideband of mode 1 and the first red sideband of mode 2. The laser addressing mode 1 has frequency $\omega_{d,1}$ with detuning from the electronic transition defined as $\delta_1^{(j)} \equiv \omega_{d,1} - \omega_{eg}^{(j)} = -2\omega_1 + \Delta$. The laser addressing mode 2 has frequency $\omega_{d,2}$, with detuning $\delta_2^{(j)} \equiv \omega_{d,2} - \omega_{eg}^{(j)} = -\omega_2 + \Delta$. Here, Δ is the common detuning of the drives from the respective sidebands. Under these conditions and within the RWA, the resulting interaction Hamiltonian takes the form:

$$\begin{aligned} \frac{\hat{V}_I^{\text{RWA}}}{\hbar} \approx & -\frac{\eta_{\text{LD},1}^2 \Omega_1}{4} \hat{\sigma}_+^{(j)} \hat{a}_1 \hat{a}_1 e^{-i\Delta t + i\phi_1} + \text{H.c.} \\ & + i \frac{\eta_{\text{LD},2} \Omega_2}{2} \hat{\sigma}_+^{(j)} \hat{a}_2 e^{-i\Delta t + i\phi_2} + \text{H.c.}, \end{aligned} \quad (20)$$

where $\hat{\sigma}_+^{(j)}$ and $\hat{\sigma}_-^{(j)}$ are the raising and lowering operators between $|g\rangle$ and $|e_j\rangle$, $\eta_{\text{LD},k}$ are the Lamb-Dicke param-

ters, Ω_k the Rabi frequencies, and ϕ_k the phases of the driving fields.

Under the condition $|\Delta| \gg \Omega_k$, the excited state can be adiabatically eliminated [84, 85] leading to an effective nonlinear coupling term:

$$\frac{\hat{H}_{\text{int}}}{\hbar} = J \left(\hat{a}_1^\dagger \hat{a}_2 + \hat{a}_2^\dagger \hat{a}_1 \right), \quad (21)$$

with coupling strength $J = \frac{\eta_{\text{LD},1}^2 \eta_{\text{LD},2} \Omega_1 \Omega_2}{8|\Delta|}$, adjustable via laser parameters. This effective coupling arises at second order through virtual excitation of the electronic state, see Supplemental Material [71].

Dissipative processes—Dissipation, as described in Eq. (2), can be engineered using sideband cooling and heating techniques [10]. For each mode individually, incoherent pumping is implemented by driving the first blue sideband, i.e. $+\omega_k$ detuning, resulting in:

$$\frac{\hat{V}_I^{\text{RWA}}}{\hbar} \approx \sum_{k=1,2} \frac{\eta_{\text{LD},k} \Omega_k}{2} \left(i \hat{\sigma}_+^{(j)} \hat{a}_k^\dagger e^{i\phi_k} + \text{H.c.} \right), \quad (22)$$

while two-phonon loss is achieved by driving the second red sideband, i.e. $-2\omega_k$ detuning:

$$\frac{\hat{V}_I^{\text{RWA}}}{\hbar} \approx - \sum_{k=1,2} \frac{\eta_{\text{LD},k}^2 \Omega_k}{4} \left(\hat{\sigma}_+^{(j)} \hat{a}_k \hat{a}_k e^{i\phi_k} + \text{H.c.} \right). \quad (23)$$

Note that the two processes described in Eqs. (22) and (23) can be independently implemented using different internal states $|e_j\rangle$. Under the assumption of rapid decay of the excited state, i.e., decay rate $\Gamma_j \gg \eta_{\text{LD},k} \Omega_k$, adiabatic elimination leads to effective dissipators in the master equation:

$$\gamma_{k,\text{eff}} \mathcal{D}[\hat{a}_k^\dagger] \hat{\rho} \quad \text{and} \quad \eta_{k,\text{eff}} \mathcal{D}[\hat{a}_k^2] \hat{\rho}, \quad (24)$$

with rates

$$\gamma_{k,\text{eff}} = \eta_{\text{LD},k}^2 \Omega_k^2 / \Gamma_j \quad \text{and} \quad \eta_{k,\text{eff}} = \eta_{\text{LD},k}^4 \Omega_k^2 / (4\Gamma_j), \quad (25)$$

controllable via laser intensities, see Supplemental Material [71].

Quantum-to-classical scaling—The crossover from quantum to classical behavior, characterized by the scaling parameter \aleph , can be explored by tuning U_k , J , and the effective dissipation rates. This tunability allows for systematic investigation of scaling laws and critical phenomena in open quantum systems. As apparent from the rescaling in Eq. (4), the classical regime corresponds to large occupations of the oscillator modes, whereas the quantum regime corresponds to low occupations.

An alternative approach to accessing the quantum-to-classical scaling involves a dual-scaling procedure of system parameters, similar to the procedure proposed in Ref. [79]. In this case, the scaling relation in Eq. (4) is replaced by the modified relation

$$\omega_k = \tilde{\omega}_k \aleph, \quad J = \tilde{J} \sqrt{\aleph}, \quad \gamma_k = \tilde{\gamma}_k \aleph \quad \text{and} \quad \hat{a}_k \rightarrow \hat{a}_k \sqrt{\aleph}. \quad (26)$$

State characterization—Trapped ion systems permit direct measurement of motional states through techniques such as Wigner function tomography [86, 87], enabling reconstruction of phase-space distributions described in Subsec. III B. While single quantum trajectories can be challenging, ensemble measurements provide access to averaged quantities, enabling comparison with the predictions discussed above.

Alternative platforms—Alternatively, the model can be realized in circuit QED using two microwave cavities, each coupled to Josephson junction elements to produce on-site Kerr nonlinearities U_k [88]. The nonlinear tunneling J is induced by a parametric pump at frequency $\omega_p = 2\omega_1 - \omega_2$, enabling three-wave mixing between the cavities [89]. Two-photon loss η_k is engineered by coupling each cavity to a lossy auxiliary mode via similar parametric drives, while incoherent pumping γ_k can be emulated either by coupling each cavity to a driven, lossy transmon qubit or by injecting broadband microwave noise into the input line [90].

Cavity optomechanical systems offer another platform, where the two dissipative modes are realized as mechanical oscillators in a “membrane-in-the-middle” setup. Here, nonlinear coupling is achieved by coupling both mechanical modes to an additional cavity mode [12, 17].

V. CONCLUSIONS

In this work, we have developed a quantum theory of limit tori (LTs), establishing a dynamical crossover that bridges open quantum dynamics and nonlinear classical dynamics. By focusing on a minimal model of two coupled driven-dissipative Kerr cavities, we systematically explored the quantum-to-classical transition using Liouvillian spectral theory and stochastic unraveling of the density matrix. Our results reveal a universal structure underlying this crossover, suggesting a broader connection between classical attractor dynamics and dissipative quantum systems.

In the classical limit, we identified robust LTs characterized by quasiperiodic motion on a toroidal phase-space manifold. Each incommensurate frequency of the torus is encoded in the Liouvillian spectrum as a pair of purely imaginary eigenvalues, corresponding to Goldstone-like modes arising from the spontaneous breaking of continuous time-translation symmetry. As quantum fluctuations increase, these eigenvalues acquire finite negative real parts, indicating the onset of quantum phase diffusion and the restoration of time-translation symmetry—a process we term quantum melting.

This quantum melting manifests as a breakdown of persistent quasiperiodicity. Through analysis of individual quantum trajectories, we identified quantum-fluctuation-induced dephasing as the microscopic mechanism driving this transition. Remarkably, even in the presence of strong noise, these trajectories remain confined to a topologically nontrivial toroidal manifold,

demonstrating the robustness of the underlying structure.

The transition is characterized by matching power-law scaling in both the Liouvillian spectral gap and a circular-variance-based order parameter, revealing a two-dimensional dynamical scaling structure in system size and time. Time itself emerges as an effective critical dimension, a hallmark of dynamical criticality reminiscent of Kosterlitz-Thouless transitions, superfluid crossovers, and scaling phenomena in low-dimensional dissipative systems. This establishes quantum melting as a continuous dissipative phase transition governed by universal scaling laws.

We further propose concrete implementations of LTs and their quantum melting in trapped ion systems and superconducting circuits, offering clear dynamical signatures and observables for detection.

Our findings contribute to a broader theoretical framework that connects topologically nontrivial attractors in classical nonlinear systems with their quantum counterparts. They also enrich current efforts to understand quantum chaos in open quantum systems [46–48, 50], where the complex structure of the Liouvillian spectrum plays a central role in signaling chaotic dynamics and their relation to classical chaos.

Together, these advances offer a path toward classifying, stabilizing, and realizing coherent quasiperiodic behavior in engineered platforms operating at the frontier between classical and quantum nonlinear dynamics. Understanding how quantum fluctuations modify classical attractors will not only deepen our theoretical understanding, but also provides insights into the design of robust quantum states for sensing, simulation, and information processing.

ACKNOWLEDGMENTS

We thank D. K. J. Boness and L. P. Peyruchat for constructive feedback on the manuscript. CN and LM acknowledge funding by the Cluster of Excellence “Advanced Imaging of Matter” (EXC 2056), Project No. 390715994. The project is co-financed by ERDF of the European Union and by “Fonds of the Hamburg Ministry of Science, Research, Equalities and Districts (BWFGB)”. KS acknowledges funding from the Deutsche Forschungsgemeinschaft (DFG) via project number 449653034.

-
- [1] P. D. Drummond and D. F. Walls, *Quantum theory of optical bistability. I. Nonlinear polarisability model*, *Journal of Physics A: Mathematical and General* **13**, 725 (1980).
 - [2] S. Aldana, C. Bruder and A. Nunnenkamp, *Equivalence between an optomechanical system and a Kerr medium*, *Physical Review A* **88**, 043826 (2013).
 - [3] N. Bartolo, F. Minganti, W. Casteels and C. Ciuti, *Exact steady state of a Kerr resonator with one- and two-photon driving and dissipation: Controllable Wigner-function multimodality and dissipative phase transitions*, *Physical Review A* **94**, 033841 (2016).
 - [4] H. Landa, M. Schiró and G. Misguich, *Multistability of Driven-Dissipative Quantum Spins*, *Physical Review Letters* **124**, 043601 (2020).
 - [5] A. M. Lyapunov, *The general problem of the stability of motion*, *International Journal of Control* **55**, 531 (1992).
 - [6] V. Sharma, *Deterministic Chaos and Fractal Complexity in the Dynamics of Cardiovascular Behavior: Perspectives on a New Frontier*, *The Open Cardiovascular Medicine Journal* **3**, 110 (2009).
 - [7] T. Laffargue, J. Tailleur and F. van Wijland, *Lyapunov exponents of stochastic systems—from micro to macro*, *Journal of Statistical Mechanics: Theory and Experiment* **2016**, 034001 (2016).
 - [8] H. Goto and T. Kanao, *Chaos in coupled Kerr-nonlinear parametric oscillators*, *Physical Review Research* **3**, 043196 (2021).
 - [9] G. Datseris and U. Parlitz, *Nonlinear Dynamics: A Concise Introduction Interlaced with Code* (Springer International Publishing, 2022).
 - [10] T. E. Lee and H. R. Sadeghpour, *Quantum Synchronization of Quantum van der Pol Oscillators with Trapped Ions*, *Physical Review Letters* **111**, 234101 (2013).
 - [11] A. Mari, A. Farace, N. Didier, V. Giovannetti and R. Fazio, *Measures of Quantum Synchronization in Continuous Variable Systems*, *Physical Review Letters* **111**, 103605 (2013).
 - [12] S. Walter, A. Nunnenkamp and C. Bruder, *Quantum synchronization of two Van der Pol oscillators*, *Annalen der Physik* **527**, 131 (2014).
 - [13] N. Lörch, E. Amitai, A. Nunnenkamp and C. Bruder, *Genuine Quantum Signatures in Synchronization of Anharmonic Self-Oscillators*, *Physical Review Letters* **117**, 073601 (2016).
 - [14] C. Davis-Tilley, C. K. Teoh and A. D. Armour, *Dynamics of many-body quantum synchronisation*, *New Journal of Physics* **20**, 113002 (2018).
 - [15] Y. Kato, N. Yamamoto and H. Nakao, *Semiclassical phase reduction theory for quantum synchronization*, *Physical Review Research* **1**, 033012 (2019).
 - [16] N. Thomas, S. Karthiga and M. Senthilvelan, *High-order synchronization in a system of nonlinearly coupled Stuart-Landau oscillators*, *The European Physical Journal Plus* **136**, 1222 (2021).
 - [17] N. Thomas and M. Senthilvelan, *Quantum synchronization in quadratically coupled quantum van der Pol oscillators*, *Physical Review A* **106**, 012422 (2022).
 - [18] C. Lu, M. Kim, Y. Yang, Y. S. Gui and C.-M. Hu, *Synchronization of dissipatively coupled oscillators*, *Journal of Applied Physics* **134** (2023), 10.1063/5.0179159.
 - [19] C. W. Wächtler and G. Platero, *Topological synchronization of quantum van der Pol oscillators*, *Physical Review Research* **5**, 023021 (2023).
 - [20] J. N. Moreno, C. W. Wächtler and A. Eisfeld, *Synchro-*

- nized states in a ring of dissipatively coupled harmonic oscillators, *Physical Review E* **109**, 014308 (2024).
- [21] D. Luo, X. Wang, D. Zhu and M. Han, *Bifurcation Theory and Methods of Dynamical Systems* (WORLD SCIENTIFIC, 1997).
- [22] H. Kielhöfer, *Bifurcation Theory: An Introduction with Applications to Partial Differential Equations* (Springer New York, 2012).
- [23] G. Floquet, *Sur les équations différentielles linéaires à coefficients périodiques*, *Annales scientifiques de l'École normale supérieure* **12**, 47 (1883).
- [24] J. P. Eckmann and D. Ruelle, *Ergodic theory of chaos and strange attractors*, *Reviews of Modern Physics* **57**, 617 (1985).
- [25] S. Strogatz, *Nonlinear dynamics and chaos*, third edition ed., A Chapman & Hall book (CRC Press, Taylor & Francis Group, Boca Raton, 2024).
- [26] A. N. Kolmogorov, *On conservation of conditionally periodic motions for a small change in Hamilton's function*, *Dokl. Akad. Nauk SSSR* **98**, 527 (1954).
- [27] J. Möser, *On invariant curves of area-preserving mappings of an annulus*, *Nachr. Akad. Wiss. Göttingen, II*, **1** (1962).
- [28] (Springer, Berlin, Heidelberg, 2009) pp. 267–294.
- [29] I. I. Yuzipov and M. V. Ivanchenko, *Quantum Neimark-Sacker bifurcation*, *Scientific Reports* **9** (2019), 10.1038/s41598-019-53526-2.
- [30] J. G. Cosme, P. Kongkhambut, A. Bölian, R. J. L. Tuquero, J. Skulte, L. Mathey, A. Hemmerich and H. Keßler, *Torus Bifurcation of a Dissipative Time Crystal*, *Physical Review Letters* **134**, 223601 (2025).
- [31] A. Garfinkel, P. S. Chen, D. O. Walter, H. S. Karagueuzian, B. Kogan, S. J. Evans, M. Karpoukhin, C. Hwang, T. Uchida, M. Gotoh, O. Nwasokwa, P. Sager and J. N. Weiss, *Quasiperiodicity and chaos in cardiac fibrillation.*, *Journal of Clinical Investigation* **99**, 305 (1997).
- [32] Y. Suzuki, M. Lu, E. Ben-Jacob and J. N. Onuchic, *Periodic, Quasi-periodic and Chaotic Dynamics in Simple Gene Elements with Time Delays*, *Scientific Reports* **6** (2016), 10.1038/srep21037.
- [33] C. Bick, M. Goodfellow, C. R. Laing and E. A. Martens, *Understanding the dynamics of biological and neural oscillator networks through exact mean-field reductions: a review*, *The Journal of Mathematical Neuroscience* **10** (2020), 10.1186/s13408-020-00086-9.
- [34] D. N. Voskresensky, *Evolution of Quasiperiodic Structures in a Non-Ideal Hydrodynamic Description of Phase Transitions*, *Universe* **6**, 42 (2020).
- [35] Y. J. F. Kpomahou, A. Adomou, J. A. Adéchinan, A. E. Yamadjako and I. V. Madogni, *Chaotic Behaviors and Coexisting Attractors in a New Nonlinear Dissipative Parametric Chemical Oscillator*, *Complexity* **2022** (2022), 10.1155/2022/9350516.
- [36] D. Zou, R. Liu, H. Liu, J. Chen, H. Dang, J. Li, A. Zhang, Y. Song, P. P. Shum and M. Hu, *Quasi-Period Dynamics of Soliton Molecules: Route to Chaos and Intrinsic Frequency Entrainment*, *Ultrafast Science* **4** (2024), 10.34133/ultrafastscience.0061.
- [37] F. Ferrari, L. Gravina, D. Eeltink, P. Scarlino, V. Savona and F. Minganti, *Steady-state quantum chaos in open quantum systems* (2023).
- [38] C. Gross and I. Bloch, *Quantum simulations with ultracold atoms in optical lattices*, *Science* **357**, 995 (2017).
- [39] F. Wilczek, *Quantum Time Crystals*, *Physical Review Letters* **109**, 160401 (2012).
- [40] D. V. Else, B. Bauer and C. Nayak, *Floquet Time Crystals*, *Physical Review Letters* **117**, 090402 (2016).
- [41] H. Keßler, J. G. Cosme, M. Hemmerling, L. Mathey and A. Hemmerich, *Emergent limit cycles and time crystal dynamics in an atom-cavity system*, *Physical Review A* **99**, 053605 (2019).
- [42] K. Seibold, R. Rota and V. Savona, *Dissipative time crystal in an asymmetric nonlinear photonic dimer*, *Physical Review A* **101**, 033839 (2020).
- [43] P. Kongkhambut, J. Skulte, L. Mathey, J. G. Cosme, A. Hemmerich and H. Keßler, *Observation of a continuous time crystal*, *Science* **377**, 670 (2022).
- [44] L. Ben Arosh, M. C. Cross and R. Lifshitz, *Quantum limit cycles and the Rayleigh and van der Pol oscillators*, *Physical Review Research* **3**, 013130 (2021).
- [45] S. Dutta, S. Zhang and M. Haque, *Quantum Origin of Limit Cycles, Fixed Points, and Critical Slowing Down*, *Physical Review Letters* **134**, 050407 (2025).
- [46] P. Zanardi and N. Anand, *Information scrambling and chaos in open quantum systems*, *Physical Review A* **103**, 062214 (2021).
- [47] T. Yoshimura and L. Sá, *Robustness of quantum chaos and anomalous relaxation in open quantum circuits*, *Nature Communications* **15** (2024), 10.1038/s41467-024-54164-7.
- [48] J. Richter, L. Sá and M. Haque, *Integrability versus chaos in the steady state of many-body open quantum systems* (2024).
- [49] P. Solanki and F. Minganti, *Chaos in Time: A Dissipative Continuous Quasi Time Crystals* (2024).
- [50] F. Ferrari, L. Gravina, D. Eeltink, P. Scarlino, V. Savona and F. Minganti, *Dissipative quantum chaos unveiled by stochastic quantum trajectories*, *Physical Review Research* **7**, 013276 (2025).
- [51] V. V. Albert and L. Jiang, *Symmetries and conserved quantities in Lindblad master equations*, *Physical Review A* **89**, 022118 (2014).
- [52] F. Minganti, A. Biella, N. Bartolo and C. Ciuti, *Spectral theory of Liouvillians for dissipative phase transitions*, *Physical Review A* **98**, 042118 (2018).
- [53] K. Macieszczak, M. Guță, I. Lesanovsky and J. P. Garrahan, *Towards a Theory of Metastability in Open Quantum Dynamics*, *Physical Review Letters* **116**, 240404 (2016).
- [54] K. Vogel and H. Risken, *Quasiprobability distributions in dispersive optical bistability*, *Physical Review A* **39**, 4675 (1989).
- [55] A. Polkovnikov, *Phase space representation of quantum dynamics*, *Annals of Physics* **325**, 1790 (2010).
- [56] C. Gardiner and P. Zoller, *The Quantum World of Ultra-Cold Atoms and Light Book I: Foundations of Quantum Optics* (IMPERIAL COLLEGE PRESS, 2014).
- [57] P. D. Drummond and B. Opanchuk, *Truncated Wigner dynamics and conservation laws*, *Physical Review A* **96**, 043616 (2017).
- [58] T. Yoneya, K. Fujimoto and Y. Kawaguchi, *Path-Integral Formulation of Truncated Wigner Approximation for Bosonic Markovian Open Quantum Systems* (2024).
- [59] F. Minganti, V. Savona and A. Biella, *Dissipative phase transitions in n -photon driven quantum nonlinear resonators*, *Quantum* **7**, 1170 (2023).

- [60] H.-P. Breuer and F. Petruccione, *The Theory of Open Quantum Systems* (Oxford University Press/Oxford, 2007).
- [61] C. W. Gardiner and P. Zoller, *Quantum noise*, 2nd ed., Springer series in synergetics No. Vol. 56 (Springer, Berlin, 2000) literaturverz. S. [419] - 425.
- [62] H. Spohn, *Approach to equilibrium for completely positive dynamical semigroups of N -level systems*, *Reports on Mathematical Physics* **10**, 189 (1976).
- [63] H. Spohn, *An algebraic condition for the approach to equilibrium of an open N -level system*, *Letters in Mathematical Physics* **2**, 33 (1977).
- [64] D. Nigro, *On the uniqueness of the steady-state solution of the Lindblad–Gorini–Kossakowski–Sudarshan equation*, *Journal of Statistical Mechanics: Theory and Experiment* **2019**, 043202 (2019).
- [65] M.-J. Hwang and M. B. Plenio, *Quantum Phase Transition in the Finite Jaynes-Cummings Lattice Systems*, *Physical Review Letters* **117**, 123602 (2016).
- [66] W. Casteels and C. Ciuti, *Quantum entanglement in the spatial-symmetry-breaking phase transition of a driven-dissipative Bose-Hubbard dimer*, *Physical Review A* **95**, 013812 (2017).
- [67] W. Casteels, R. Fazio and C. Ciuti, *Critical dynamical properties of a first-order dissipative phase transition*, *Physical Review A* **95**, 012128 (2017).
- [68] R. Puebla, M.-J. Hwang, J. Casanova and M. B. Plenio, *Probing the Dynamics of a Superradiant Quantum Phase Transition with a Single Trapped Ion*, *Physical Review Letters* **118**, 073001 (2017).
- [69] M.-J. Hwang, P. Rabl and M. B. Plenio, *Dissipative phase transition in the open quantum Rabi model*, *Physical Review A* **97**, 013825 (2018).
- [70] C. Lledó, T. K. Mavrogordatos and M. H. Szymańska, *Driven Bose-Hubbard dimer under nonlocal dissipation: A bistable time crystal*, *Physical Review B* **100**, 054303 (2019).
- [71] See Supplemental Material for additional details.
- [72] A. L. Schawlow and C. H. Townes, *Infrared and Optical Masers*, *Physical Review* **112**, 1940 (1958).
- [73] A. Chia, M. Hajdušek, R. Fazio, L.-C. Kwek and V. Vedral, *Phase diffusion and the small-noise approximation in linear amplifiers: Limitations and beyond*, *Quantum* **3**, 200 (2019).
- [74] Y. Hidaka and Y. Minami, *Spontaneous symmetry breaking and Nambu–Goldstone modes in open classical and quantum systems*, *Progress of Theoretical and Experimental Physics* **2020** (2020), 10.1093/ptep/ptaa005.
- [75] S. Strogatz, *Nonlinear dynamics and chaos*, second edition, first issued in hardback ed., A Chapman & Hall book (CRC Press, Boca Raton, 2019) literaturverzeichnis: Seite 470-482.
- [76] N. Goldenfeld, *Lectures on phase transitions and the renormalization group*, The @advanced book program (CRC Press, Taylor & Francis Group, Boca Raton, 2018) includes bibliographical references and index.
- [77] H. Alaeian, G. Giedke, I. Carusotto, R. Löw and T. Pfau, *Limit cycle phase and Goldstone mode in driven dissipative systems*, *Physical Review A* **103**, 013712 (2021).
- [78] K. Ptaszyński and M. Esposito, *Dynamical signatures of discontinuous phase transitions: How phase coexistence determines exponential versus power-law scaling*, *Physical Review E* **110**, 044134 (2024).
- [79] G. Beaulieu, F. Minganti, S. Frasca, V. Savona, S. Felicetti, R. Di Candia and P. Scarlino, *Observation of first- and second-order dissipative phase transitions in a two-photon driven Kerr resonator*, *Nature Communications* **16**, 1954 (2025).
- [80] J. Steinbach, J. Twamley and P. L. Knight, *Engineering two-mode interactions in ion traps*, *Physical Review A* **56**, 4815 (1997).
- [81] M. Kajita, *Ion Traps*, 1st ed., IOP Ebooks Series (Institute of Physics Publishing, Bristol, 2022) description based on publisher supplied metadata and other sources.
- [82] G. S. Agarwal and J. Banerji, *Fractional revivals in systems with two time scales*, *Physical Review A* **57**, 3880 (1998).
- [83] J. Walz, I. Siemers, M. Schubert, W. Neuhauser, R. Blatt and E. Teloy, *Ion storage in the rf octupole trap*, *Physical Review A* **50**, 4122 (1994).
- [84] J. I. Cirac, R. Blatt, P. Zoller and W. D. Phillips, *Laser cooling of trapped ions in a standing wave*, *Physical Review A* **46**, 2668 (1992).
- [85] F. Reiter and A. S. Sørensen, *Effective operator formalism for open quantum systems*, *Physical Review A* **85**, 032111 (2012).
- [86] S. Ding, G. Maslennikov, R. Hübner, H. Loh and D. Matsukevich, *Quantum Parametric Oscillator with Trapped Ions*, *Physical Review Letters* **119**, 150404 (2017).
- [87] L. G. Lutterbach and L. Davidovich, *Method for Direct Measurement of the Wigner Function in Cavity QED and Ion Traps*, *Physical Review Letters* **78**, 2547 (1997).
- [88] T. Hillmann and F. Quijandría, *Designing Kerr Interactions for Quantum Information Processing via Counterrotating Terms of Asymmetric Josephson-Junction Loops*, *Physical Review Applied* **17**, 064018 (2022).
- [89] R. Lescanne, M. Villiers, T. Peronnin, A. Sarlette, M. Delbecq, B. Huard, T. Kontos, M. Mirrahimi and Z. Leghtas, *Exponential suppression of bit-flips in a qubit encoded in an oscillator*, *Nature Physics* **16**, 509 (2020).
- [90] A. Narla, S. Shankar, M. Hatridge, Z. Leghtas, K. Sliwa, E. Zalys-Geller, S. Mundhada, W. Pfaff, L. Frunzio, R. Schoelkopf and M. Devoret, *Robust Concurrent Remote Entanglement Between Two Superconducting Qubits*, *Physical Review X* **6**, 031036 (2016).